EPJ Nuclear Sci. Technol. **11**, 7 (2025)
© Y. Jo and D. Lee, Published by EDP Sciences, 2025
https://doi.org/10.1051/epjn/2025001

EPJ Nuclear Sciences & Technologies

Available online at:
https://www.epj-n.org

Status and advances of Monte Carlo codes for particle transport simulation, edited by Andrea Zoia, Cheikh Diop and Cyrille de Saint Jean

REGULAR ARTICLE

OPEN ACCESS

Current capabilities and future developments of Monte Carlo code MCS

Yunki Jo[1] and Deokjung Lee[1,2,*]

[1] Department of Nuclear Engineering, Ulsan National Institute of Science and Technology, 50 UNIST-gil, Eonyang-eup, Ulju-gun, Ulsan 44919, Republic of Korea
[2] Advanced Nuclear Technology and Services, 406-21 Jonga-ro, Jung-gu, Ulsan 44429, Republic of Korea

Received: 18 August 2024 / Received in final form: 28 January 2025 / Accepted: 30 January 2025

Abstract. The Monte Carlo code, MCS was developed at the Ulsan National Institute of Science and Technology (UNIST) in 2011. In the initial development phase, the primary focus was on developing a Monte Carlo code for the high-fidelity multicycle analysis of large-scale power reactors, especially pressurized water reactors. For the power reactor analysis, capabilities including refueling and shuffling of fuel assemblies, on-the-fly Doppler broadening of neutron cross-sections, and multiphysics coupling were implemented in the MCS. Beyond reactor analysis and capabilities, MCS has been developed to extend its applications. The MCS has been used for radiation shielding, group constants generation, sensitivity, uncertainty, and transient analysis. This study provides a general overview of MCS capabilities.

1 Introduction

The Monte Carlo method [1], widely used for nuclear reactor analysis due to advances in computing power, simulates particle histories with pseudo-random numbers to achieve statistically converged results. It uses high-fidelity physics phenomena through stochastic particle simulations and models exact problem geometries. Since 2011, the Monte Carlo neutron and photon transport code MCS has been developed at the Ulsan National Institute of Science and Technology (UNIST) [2]. Over the past decade, in addition to high-fidelity multicycle power reactor analysis, MCS has incorporated essential features for group constants generation, radiation shielding analysis, and sensitivity and uncertainty (S/U) analysis. Figure 1 illustrates the representative capabilities of Monte Carlo code MCS, which are detailed in this paper.

2 Capabilities of Monte Carlo code MCS

2.1 Neutron and photon transport capability

The constructive solid geometry (CSG) system was used to model the complex geometries in the MCS. Users can define universes and lattices to efficiently model the repeated geometries of the fuel rods and assemblies in reactor cores. MCS automatically checks for undefined or overlapping cells in the input file to prevent tracking failures due to human errors. It also supports input and output visualization as a PPM-formatted image file. Figure 2 shows radial and axial images of the 3-D reactor core model generated by MCS. MCS can visualize output data, such as nuclide density of depleted materials, temperature, weight-window map, and tally results, by overlaying them on the input geometry.

MCS supports both criticality and fixed-source modes, with neutron transport capabilities covering an energy range of 10^{-11} MeV to 20 MeV. It reads the ACE-format (A Compact ENDF) cross-section data [3] from nuclear data libraries such as ENDF/B, JENDL, and JEFF. The $S(\alpha, \beta)$ neutron thermal scattering cross-section is used for low energy scattering with key moderator nuclides such as hydrogen in water and carbon in graphite. Probability table data are available for unresolved energy ranges, and On-the-fly Doppler broadening of the neutron cross-section is used to account for temperature changes via thermal/hydraulic feedback in high-fidelity reactor analysis. In the resolved resonance energy range, MCS calculates Doppler-broadened cross-sections using a multipole representation [4] and the windowed multipole method, implemented with an OpenW module provided by MIT [5] to UNIST. Linear-linear and log-linear interpolation schemes are used for thermal scattering and probability table data, respectively, as they were used in the *makxsf* code [6].

MCS includes an unpolarized photon transport simulation for photon energies ranging from 1 keV to 20 MeV, covering elements from $Z = 1$ (hydrogen) to $Z = 100$

* e-mail: deokjung@unist.ac.kr

This is an Open Access article distributed under the terms of the Creative Commons Attribution License (https://creativecommons.org/licenses/by/4.0), which permits unrestricted use, distribution, and reproduction in any medium, provided the original work is properly cited.

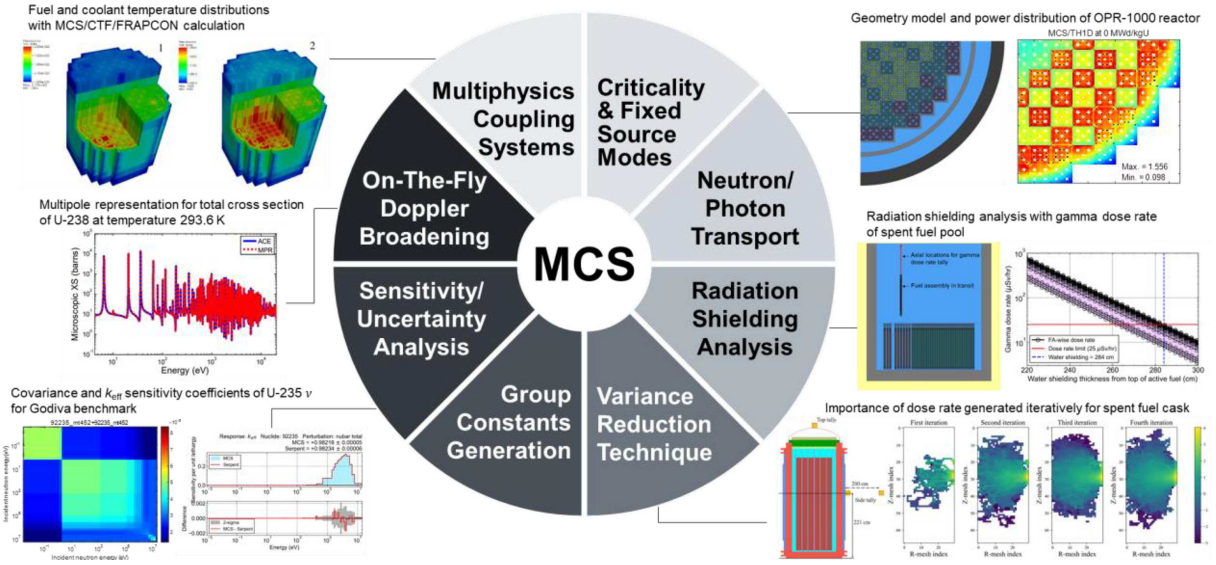

Fig. 1. Representative capabilities of Monte Carlo code MCS.

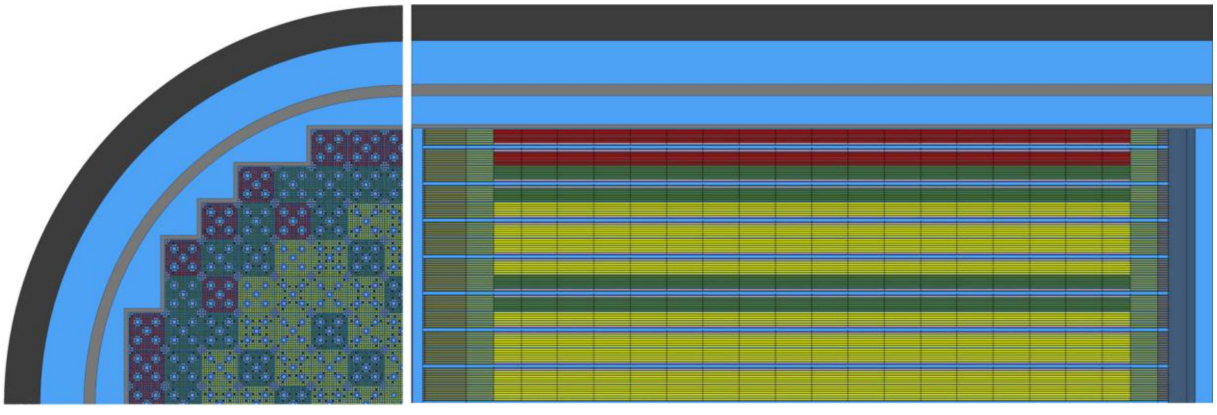

Fig. 2. Radial (left) and axial (right) images of 3-D reactor core model generated by MCS.

(fermium) [7]. Photon transport can be simulated in both photon-only and coupled neutron-photon transport modes. The simulation models four key photon interactions: the photoelectric effect, Compton scattering, electron-positron pair production, and Rayleigh scattering. Additionally, it accounts for three secondary photon production processes: positron annihilation at rest, atomic relaxation, and electron/positron bremsstrahlung.

The MCS input file uses an extensible markup language (XML) format, where the input values are paired with the XML tags or keywords. Figure 3 shows an XML-based input file for the Godiva benchmark. MCS supports C and Python preprocessors. C pre-processor definitions (#define, #ifdef) and Python scripts can be written in the MCS input file. MCS output files are provided in MATLAB-readable m-file and Python-readable py-file formats, facilitating easy post-processing. MCS also supports parallel simulations using MPI, OpenMP, and hybrid MPI/OpenMP approaches. To minimize communication overhead in large-scale simulations, MCS implements the parallel fission bank algorithm from OpenMC [8].

2.2 Features for a high-fidelity reactor analysis

MCS includes essential features for high-fidelity power reactor analysis, such as depletion calculation, a quadratic depletion model for gadolinium isotopes, equilibrium xenon function, thermal/hydraulic feedback, soluble boron concentration search, and control rod position search capabilities. The adjoint-weighted point kinetics parameter calculation using the iterated fission probability (IFP) method [9] is available. Time-dependent Monte Carlo (TDMC) capability for transient analysis is under development [10], with initial simulations performed for the C5G7-TD benchmark. TDMC acceleration is needed for large-scale commercial reactors. A functional expansion tally (FET) capability was developed in MCS to produce continuous representations of tallied quantities [11]. Preliminary FET results for a hypothetical 2×2 pin problem demonstrated that MCS could generate smooth, continuous power distributions using FET. Further development for high-fidelity reactor analysis is ongoing.

The Chebyshev rational approximation method (CRAM) solver [12] was implemented in MCS to solve

```
<mcs>
    <surface name="s1" type="sphere" coeffs="0 0 0 8.7407" boundary="black" />

    <cell name="c1" material="fuel" zone=" -s1 " />

    <material name="fuel" units="#/barn-cm"  >
        <nuclide id="92234" ratio=" 4.9184E-04" />
        <nuclide id="92235" ratio=" 4.4994E-02" />
        <nuclide id="92238" ratio=" 2.4984E-03" />
    </material>

    <source>
        <scell shape="point" coeffs="0 0 0"/>
    </source>

    <criticality active="400" inactive="50" history="100000" />
</mcs>
```

Fig. 3. MCS input file of XML format for Godiva benchmark.

the Bateman equation, using radioactive decay and fission yield data from ENDF-format nuclear data libraries. By default, 1373 nuclides are considered in depletion calculations, with an option for 3820 nuclides. Effective one-group cross-sections are tallied in a transport calculation for material transmutation. MCS offers three burnup strategies: predictor, semi-predictor-corrector, and full predictor-corrector methods. The semi-predictor-corrector and complete predictor-corrector methods used in MCS are called the Ce/BE and CE/BE algorithms, respectively [13]. Both Ce and CE mean constant extrapolation for the predictor step. The Ce uses cross-sections and flux from the previous step without solving the current step. On the other hand, the CE uses cross-sections and flux from the current state after solving it. The BE represents a backward extrapolation for the corrector step by averaging atomic densities from current and previous states. MCS includes a quadratic depletion model for Gd isotopes [14], allowing larger depletion step sizes for Gd-bearing fuel assemblies without sacrificing accuracy, despite the high-absorption cross-sections of Gd-155 and Gd-157. To address potential unphysical neutron flux oscillations caused by the high-absorption cross-section of Xe-135, MCS implements an equilibrium xenon calculation function [15], updating the Xe-135 number density at each transport cycle using tallied neutron flux and reaction rates.

MCS includes fuel assembly-wise refueling and shuffling capabilities. When refueling is selected, MCS generates depleted material files for each fuel assembly at each depletion step. These files can be directly used as input for the next reactor cycle without further post-processing.

During reactor analysis, the fuel and coolant temperature distributions depend on the reactor power distribution. MCS incorporates the TH1D solver [16], for 1-D single-phase closed-channel thermal/hydraulics analysis. Using pin-wise axial power distributions tallied during a neutron transport cycle, the TH1D solver computes temperature distributions for fuel, cladding, and coolant, as well as coolant density distribution. The axial temperature profile is derived from steady-state mass and energy conservation equations, solved from the bottom to the top of the fuel rod. A finite-difference method was used to solve steady-state cylindrical heat conduction equations with energy balance constraints for radial temperature distribution in each axial node. In TH1D calculations, a single-phase coolant in a closed channel is assumed, so cross-flow between channels is not considered. Thermal/hydraulics feedback accounting for cross-flow is available through multiphysics coupling with COBRA-TF (CTF) [17]. The following section presents the thermal/hydraulic feedback results from TH1D and CTF. In MCS, the batching method [18] has been implemented to reduce the inter-cycle correlation of Monte Carlo calculation. In the batching method, a single batch consists of one or multiple cycles. The final results and statistical uncertainties are calculated over batches. As the number of cycles per batch increases, the inter-cycle correlation decreases.

MCS includes soluble boron concentration and control rod position search capabilities to manage reactor criticality and control the excess reactivity of commercial reactors. The soluble boron concentration search capability is widely used in commercial PWR analyses to determine critical boron levels, while the control rod position search capability is applied in boron-free small modular reactor analyses. In MCS input files, users can set a target k-eigenvalue, B-10 ratio in soluble boron, control rod bank positions, insertion order, and overlapping positions. Soluble boron concentration and control rod positions are updated each transport cycle based on the k-eigenvalue at a current cycle. To ensure accurate results, sufficient inactive cycles are needed for convergence of boron concentration and control rod positions before the active cycle begins. MCS output files include the average and statistical error of soluble boron concentration, control rod positions, and k-eigenvalue results. The critical control rod position was determined for a 17×17 Westinghouse fuel assembly model with 3.1 wt.% enrichment. Reflective boundary conditions were applied in the x- and y-directions, and a black boundary condition in the z-direction. For simplicity, B_4C rods were assumed to be inserted into all guide and instrument tubes of the fuel assembly. The initial control rod position was fully

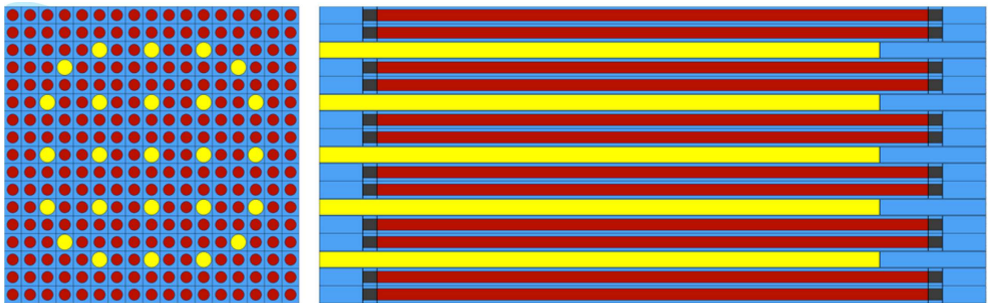

Fig. 4. Control rod insertion positions (left) and searched critical control rod position (right).

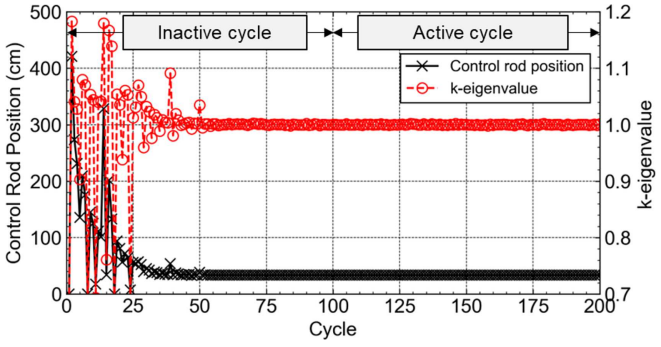

Fig. 5. Iterative control rod position search results.

inserted. MCS calculation used 100 inactive and 100 active cycles with one million histories per cycle. The critical control rod position was found to be 33.44 cm, as shown in Figure 4, with iterative position updates depicted in Figure 5. The control rod position converges to 33.44 cm at the 60th inactive cycle. The calculated k-eigenvalue is 1.00010 ± 0.00008.

The MCS reactor analysis capability has been verified and validated through various benchmarks, including the BEAVRS [2], VERA [19,20], international criticality safety benchmark experimental problems (ICSBEP) [21, 22], NUREG/CR-6361 critical experiments [23], VVER-1000 mock-up criticality experiments [24], and China experimental fast reactor (CEFR) [25]. MCS also supports modelling randomly distributed tristructural-isotropic (TRISO) particle fuel for high-temperature gas-cooled reactors and was used to analyze HTR-PM, a high-temperature gas-cooled pebble-bed reactor in China containing TRISO particle fuels. [26].

Figure 6 shows the normalized pin power distributions from the MCS/TH1D calculation for OPR-1000 at the beginning of the cycle (BOC), middle of the cycle (MOC), and end of the cycle (EOC). Statistical errors for tallied pin powers were below 1%, except in peripheral regions, where they increased to 2% due to lower pin powers. The next section will present results for critical boron concentration (CBC), fuel temperature, and coolant temperature distributions, comparing MCS/TH1D results with multiphysics coupled calculations. The whole core calculations in Sections 2.2 and 2.3 used 30 active batches with 300 cycles per batch and 20,000 histories per cycle to minimize the inter-cycle correlation.

2.3 Multiphysics coupling capability

A Multiphysics coupling system integrating neutronics, thermal-hydraulics, and fuel-performance codes has been developed for large-scale high-fidelity reactor analysis with MCS [27–31]. MCS is coupled with CTF [17] for thermal/hydraulics and FRAPCON-4.0 [32] for fuel performance calculations. CTF, the CASL version of COBRA-TF, is a 3-D sub-channel thermal/hydraulics code using a two-fluid model to simulate three separate fluid fields: liquid films, droplets, and vapor. This solves mass, momentum, and energy conservation equations. The cross-flow between fuel rod channels is simulated through multiphysics coupled with the CTF. FRAPCON, developed by the Pacific Northwest National Laboratory (PNNL), is a 1-D fuel performance code that calculates the steady-state response of oxide fuel rods in light-water reactors, including temperature, pressure, and deformation of the fuel rod.

Figure 7 illustrates the flowchart for the MCS/CTF/FRAPCON multiphysics coupled calculation. The 3-D power distribution is tallied in MCS neutron transport calculations and then transferred to CTF and FRAPCON for updates to coolant and fuel temperatures, respectively. Thermal/hydraulics CTF calculations update coolant temperature and density, which are then passed to FRAPCON. Single-rod calculations of FRAPCON update the temperatures of fuel, gap, and cladding. Finally, these updated temperature and density distributions are sent back to MCS to refine the cross-section data in neutron transport calculations. Thermal/hydraulics feedback occurs once per transport cycle in this coupled system.

Figure 8 presents the CBC results and differences among the multiphysics coupled MCS calculations, namely MCS/TH1D, MCS/FRAPCON, and MCS/CTF, for the OPR-1000 reactor. The error bars represent the 1-σ statistical error of the CBC results. However, they are too small to be checked in the left figure of Figure 8. CBC differences between MCS/TH1D and MCS/CTF are generally below 3 ppm, except for a 7.2 ppm difference at 12 MWd/kgU, indicating that the cross-flow effect from CTF has minimal impact on core reactivity. However, CBC differences between MCS/FRAPCON and MCS/TH1D are −9.2 ppm at BOC, attributed to higher fuel temperatures in MCS/FRAPCON. Figures 9 and 10 show the fuel temperature distributions from multiphysics coupled MCS

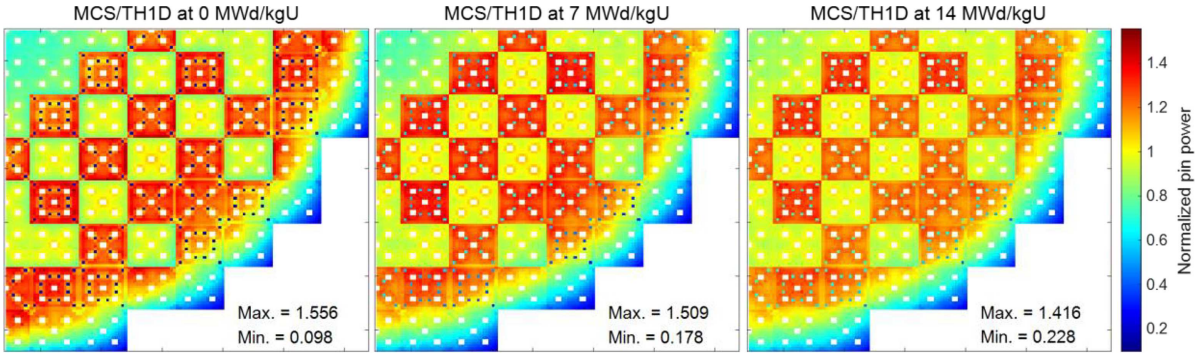

Fig. 6. Normalized pin power distribution of MCS/TH1D for OPR-1000.

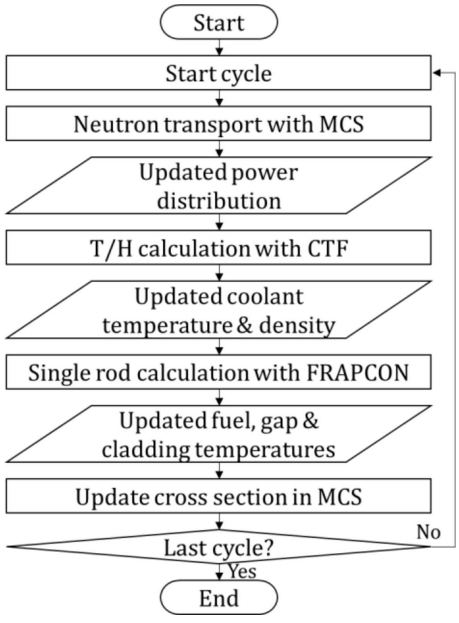

Fig. 7. Flow chart of MCS/CTF/FRAPCON multiphysics coupled calculation.

calculations for the OPR-1000 reactor at BOC and EOC, respectively. At BOC, MCS/FRAPCON has higher fuel temperatures compared to MCS/TH1D and MCS/CTF, while at EOC, its temperatures are lower. This variation is due to the dynamic gap conductance model in FRAPCON. Figure 11 shows the gap conductance results of the multiphysics coupled systems for OPR-1000. The error bars represent the 1-σ statistical error of the gap conductance results. MCS/TH1D and MCS/CTF use a fixed gap conductance of 10,000 W/m^2-K regardless of the fuel burnup. In contrast, the MCS/FRAPCON coupled system adjusts gap conductance based on burnup, temperature, and gas pressure. At BOC, the gap conductance of MCS/FRAPCON is lower than the fixed-gap conductance value used in MCS/TH1D and MCS/CTF, but it exceeds it at EOC.

Figures 12 and 13 present the coolant temperature distributions of the multiphysics coupled MCS calculations for OPR-1000 at BOC and EOC, respectively. The CTF distribution shows realistic cross-flow between adjacent channels, while the MCS/TH1D and MCS/FRAPCON calculations, based on closed single-channel models for the thermal/hydraulic feedback, do not exhibit this cross-flow effect.

2.4 Group constants generation capability

Few-group constants generation capability was implemented in the MCS for reactor analysis using a two-step transport/nodal diffusion method [33–36]. In this approach, transport calculations generate the few-group constants of the fuel assemblies which are then used by a nodal diffusion code for reactor analysis. This method is popular owing to the short computation time of the nodal diffusion code. Deterministic lattice transport codes are commonly employed to generate few-group constants for fuel assemblies. However, deterministic transport codes contain inherent errors due to spatial, energy, and angular discretization. To address this, Monte Carlo codes generate few-group constants using a two-step approach. MCS was also used to produce homogenized group constants for the nodal diffusion codes RAST-K and PARCS. The k-eigenvalue and power distribution results from MCS/RAST-K and MCS/PARCS were compared with MCS standalone results for fast [33–35] and light water reactors [36], respectively. The accuracy of critical spectrum computing methods —B1, P1, and CASMO-4E (CM)—was evaluated, in addition to the inflow and outflow transport corrector methods. In the WBN1 benchmark problems, the inflow transport correction combined with the CM method showed the most minor error among all test cases [36].

2.5 Radiation shielding analysis using the weight window method

For radiation shielding analysis, the weight window (WW) method was implemented in the MCS [37], a common variance-reduction technique for deep-penetration shielding problems. In WW simulations, particles are split or removed based on WW boundaries, which are determined by the importance of the target response. This increases the number of particles entering a high-importance region

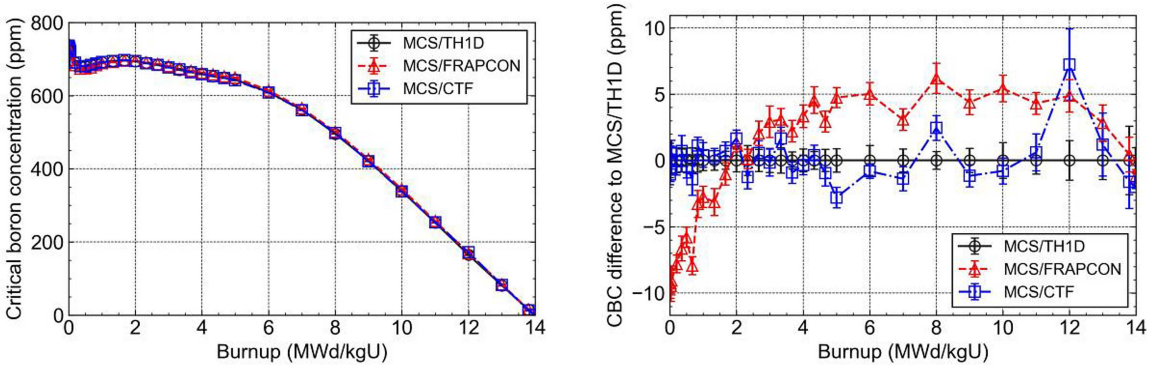

Fig. 8. Critical boron concentration results (left) and difference (right) among multiphysics coupled MCS calculations for OPR-1000 reactor.

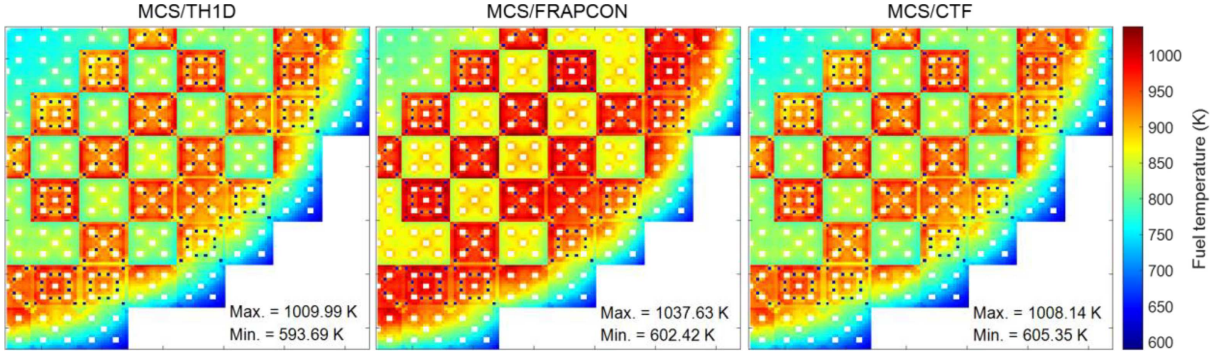

Fig. 9. Fuel temperature distribution of multiphysics coupled MCS calculations for OPR-1000 at the beginning of a cycle.

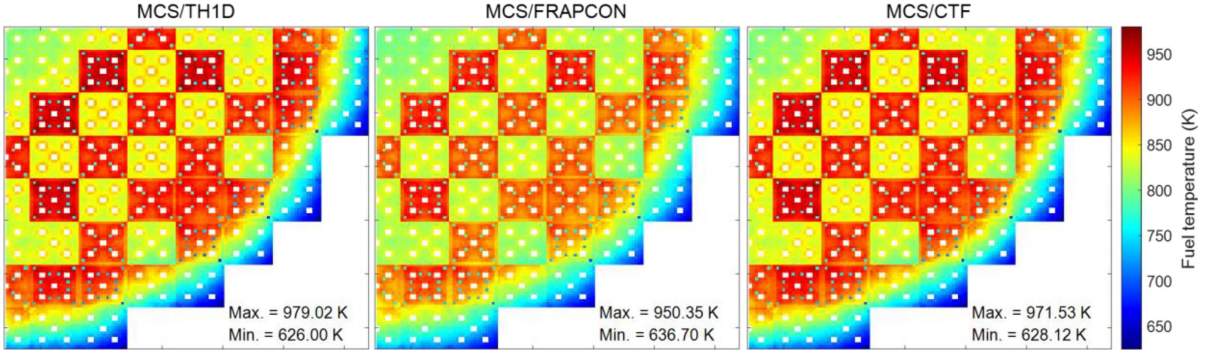

Fig. 10. Fuel temperature distribution of multiphysics coupled MCS calculations for OPR-1000 at the end of a cycle.

through a particle split and reduces it in a low-importance region by the particle removal of the Russian roulette. Consequently, more particles are simulated near the target tally position and smaller statistical errors are obtained. Additionally, 10 statistical tests were incorporated into MCS to validate the tally results for shielding problems [38].

MCS was applied in the radiation shielding analysis of spent fuel casks [39], shielding integral benchmark archive and database (SINBAD) [40,41], and spent fuel pools [42]. A fixed-source mode simulation and weight window technique with 10 statistical tests were used for dose rate calculations. Figure 14 illustrates the spent fuel pool model and the gamma dose rate results for the assembly in transit as a function of water-shielding thickness. The error bars represent the 1-σ statistical error of the gamma dose rate results. The gamma dose rates were calculated for each fuel assembly in the reactor core at the end of the cycle. The fuel assembly-wise gamma dose rate results were influenced by fuel enrichment, assembly burnup, power history, and cooling time. It was calculated by multiplying the photon flux by the photon flux-to-dose conversion factor, derived using ICRP-116 [43] with log-log interpolation. The required water shielding thickness to reduce the radiation dose rate at the spent fuel pool surface below 25 μSv/hr [44,45] was calculated as 284 cm, shown as a vertical dashed line in Figure 14. All tally results in Figure 14 passed 10 statistical tests. The

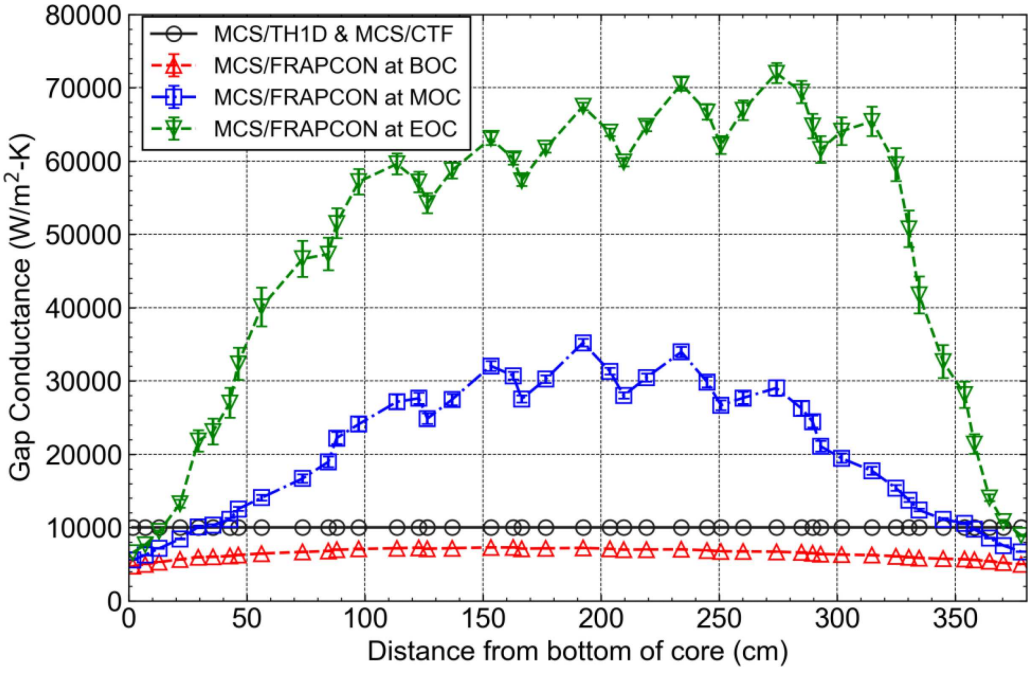

Fig. 11. Radially averaged gap conductance of multiphysics coupled MCS calculations for OPR-1000.

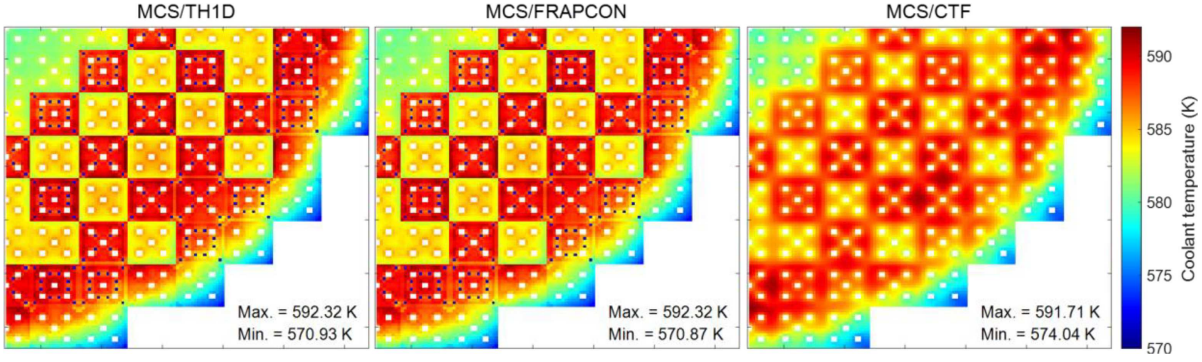

Fig. 12. Coolant temperature distribution of multiphysics coupled MCS calculations for OPR-1000 at the beginning of a cycle.

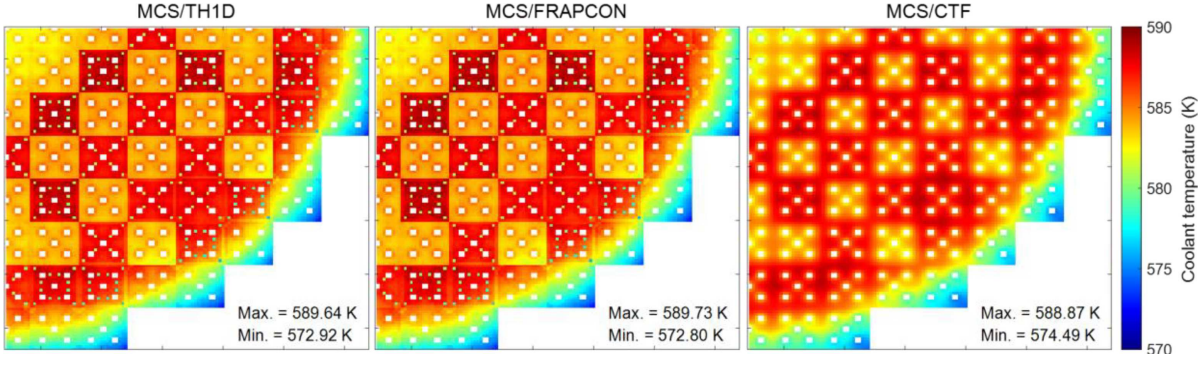

Fig. 13. Coolant temperature distribution of multiphysics coupled MCS calculations for OPR-1000 at the end of a cycle.

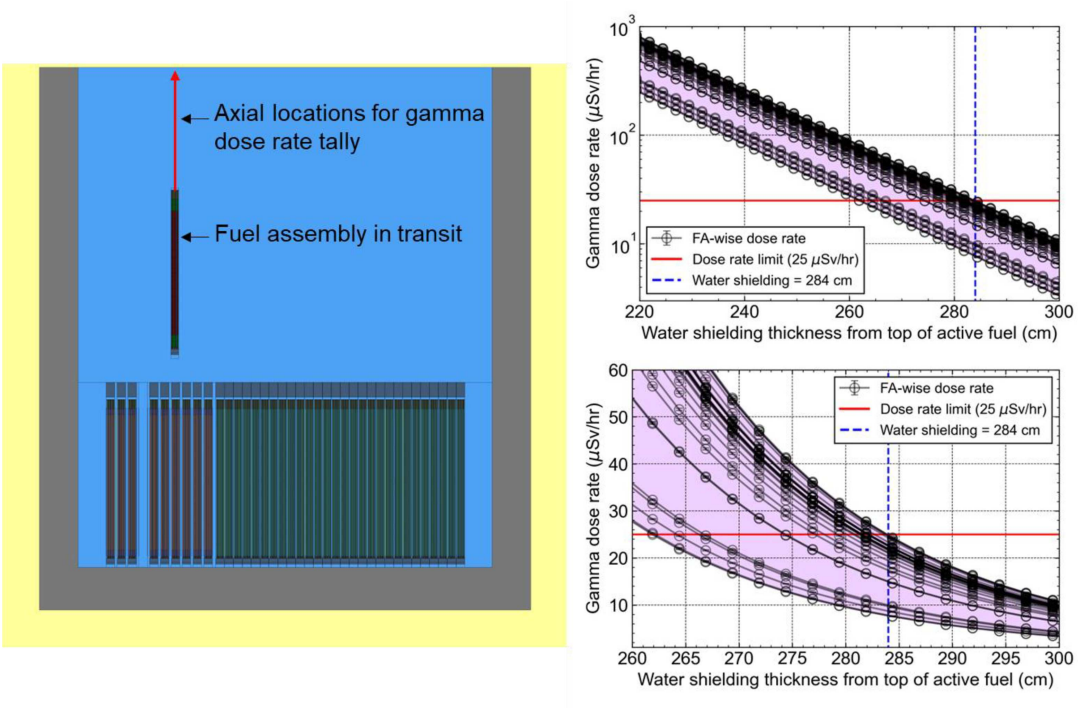

Fig. 14. Spent fuel pool model (left) and gamma dose rate results (right) of assembly in transit depending on the thickness of water shielding in the spent fuel pool.

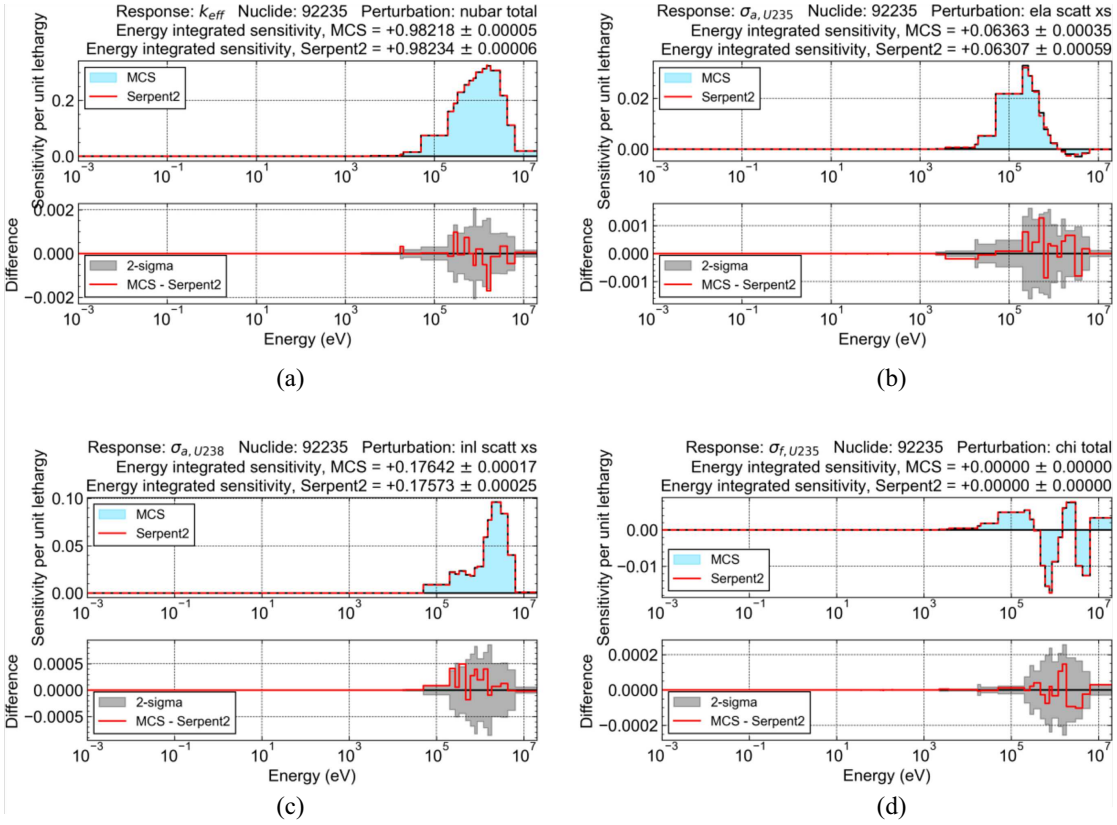

Fig. 15. Comparison of sensitivity coefficients between MCS and Serpent2 for Godiva benchmark. (a) k_{eff} sensitivity to U-235 $\bar{\nu}_{\mathrm{total}}$, (b) $\sigma_{\mathrm{a,U235}}$ sensitivity to U-235 σ_{ela}, (c) $\sigma_{\mathrm{a,U238}}$ sensitivity to U-235 σ_{inl}, (d) $\sigma_{\mathrm{f,U235}}$ sensitivity to U-235 χ_{total}.

WW method increased the figure of merit (FOM) of the gamma dose rate at a 209.38 cm water shielding thickness by approximately 30,000 times, with greater increases at thicker shielding locations.

2.6 Sensitivity and uncertainty analysis using perturbation theory

The S/U analysis capability was implemented in MCS [46,47] to establish confidence bounds for nuclear reactor safety analysis and design by uncertainty propagation from nuclear data [48]. MCS computes sensitivity coefficients of k-eigenvalue and reaction rate ratio using generalized perturbation theory [49,50] and the IFP method [9]. The uncertainties are quantified by multiplying the sensitivity coefficients with covariance data from the nuclear data library using a sandwich rule. MCS has been applied in S/U analysis for OECD/NEA uncertainty analysis for modelling the benchmarks of light water reactors (UAM-LWRs) and sodium-cooled fast reactors (UAM-SFRs) [46,47], analyzing uncertainties in k-eigenvalue, microscopic, and macroscopic cross-sections by comparing top contributors.

The IFP method used for the S/U analysis requires a substantial memory, proportional to the number of histories, to store tally quantities of each neutron history in the original generation. To mitigate this, a super-history method [51,52] and the Wielandt method [53,54] were implemented in MCS, effectively reducing memory demands.

Figure 15 shows the sensitivity coefficients of $k$eigenvalue, $\sigma_{a,U235}$, $\sigma_{a,U235}$, and $\sigma_{f,U235}$ for the Godiva benchmark, with MCS results closely matching Serpent2 [55], with differences within 2-σ statistical errors. The value above each graph represents the energy integrated sensitivity coefficient. It represents the fractional change of a target response due to the input parameters perturbed in the entire energy range. The U-235 fission cross-section sensitivity to U-235 total fission neutron spectrum (χ_{total}) is shown in Figure 15-d. The fission neutron spectrum is always normalized to unity, and the implicit normalization is introduced as a constraint in the sensitivity calculation. The energy integrated sensitivity coefficient results of MCS and Serpent2 are zero due to the constrained condition of the fission neutron spectrum [56].

A recently developed adjoint flux calculation technique, the perturbation-included iterated fission probability (PIFP) method, enables the exact perturbation theory in Monte Carlo transport [57]. The PIFP method computes the adjoint flux of a perturbed system during forward Monte Carlo simulation of an unperturbed system, facilitating the application of exact perturbation theory in forward calculations. Both the PIFP and exact perturbation methods were implemented in MCS. Figure 16 shows the results for the boron concentration changes in the PLUS7 fuel assembly, with the exact perturbation (EP) method demonstrating significantly improved accuracy over conventional linear perturbation methods such as differential operator sampling (DOS) and adjoint-weighted perturbation (AWP).

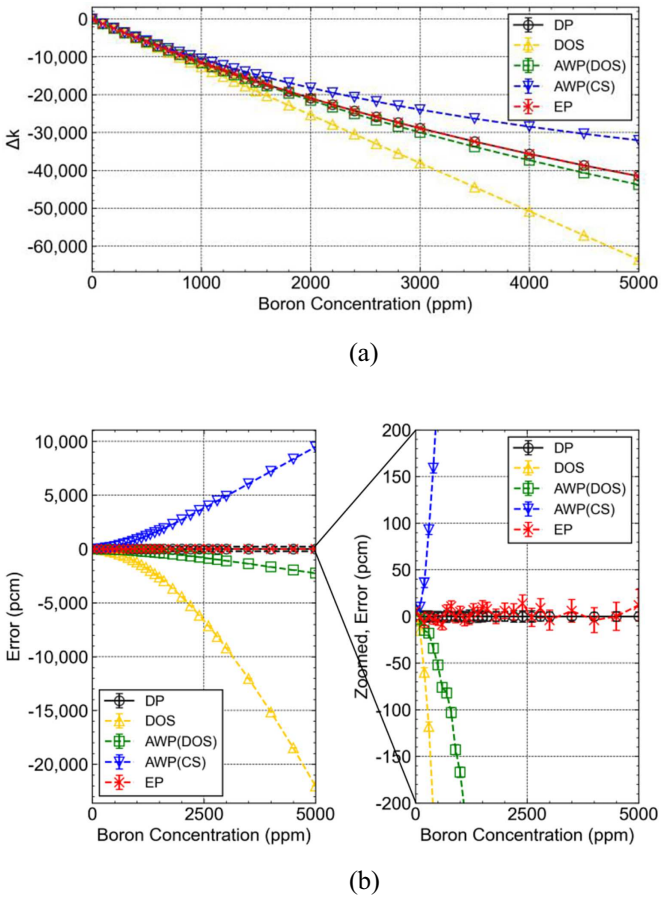

Fig. 16. Results of perturbation methods for boron concentration change in PLUS7 fuel assembly. (a) k-eigenvalue change. (b) Error in the estimated k-eigenvalue.

3 Conclusion

This paper provides an overview of MCS, highlighting its power reactor analysis capabilities, including depletion calculation, on-the-fly Doppler broadening of neutron cross-sections, multiphysics coupling, refueling and shuffling of fuel assemblies, soluble boron concentration, and control rod position search. Multiphysics coupling results for the OPR-1000 reactor are presented, comparing critical boron concentration, fuel and coolant temperature distributions, and gap conductance. Beyond reactor analysis capabilities, MCS has been extended to applications, including group constants generation, radiation shielding analysis, and S/U analysis. Gamma dose rate results for the spent fuel pool were presented for radiation shielding analysis, showing a more than 30,000-fold increase in FOM using the WW variance reduction technique. Sensitivity coefficients from generalized perturbation theory in MCS were demonstrated for the Godiva benchmark and verified by comparison with Serpent2 results.

MCS development is ongoing, focusing on optimizing, accelerating, and expanding its capabilities. The recently developed PIFP method for EP in Monte Carlo transport, implemented alongside the EP method in MCS, has shown significantly improved accuracy over conventional

perturbation methods like DOS and AWP. FET capability now allows for continuous distributions of neutron flux, temperature, and power in high-fidelity reactor analysis. Acceleration of the TDMC method is needed for transient analysis of large-scale commercial reactors. Additional developments include thermal expansion modelling for reactor geometry and the use of AI to cluster fuel rods, reducing the computational load in high-fidelity analyses.

Funding

This work was partially supported by the Energy Efficiency & Resources of the Korea Institute of Energy Technology Evaluation and Planning(KETEP) grant funded by the Ministry of Trade, Industry and Energy(No. 20224B10100130). This work was partially supported by the Innovative Small Modular Reactor Development Agency grant funded by the Korean government (MOTIE; No. RS-2024-00407975). This work was partially supported by the National Research Foundation of Korea (NRF) grant funded by the Korean government (MSIT). (No. NRF-2019M2D2A1A03058371).

Conflicts of interest

The authors declare no conflict of interest.

Data availability statement

No data are associated with this article.

Author contribution statement

Yunki Jo: Conceptualization, Formal analysis, Methodology, Software, Validation, Visualization, Writing - Original draft. Deokjung Lee: Conceptualization, Supervision, Project administration, funding acquisition, Writing - Review, and editing.

References

1. F.B. Brown, T.M. Sutton, *Monte Carlo fundamentals. No. KAPL-4823* (Knolls Atomic Power Lab. (KAPL), Niskayuna, NY (United States), 1996)
2. H. Lee, W. Kim, P. Zhang, M. Lemaire, A. Khassenov, J. Yu, Y. Jo, J. Park, K. Lee, MCS – A Monte Carlo particle transport code for large-scale power reactor analysis, Ann. Nucl. Energy **139**, 107276 (2020)
3. X-5 Monte Carlo Team, *MCNP–A General Monte Carlo N-Particle Transport Code, Version 5. LA-UR-03-1987* (Los Alamos National Laboratory, 2003)
4. A. Khassenov, S. Choi, D. Lee, On the fly doppler broadening using multipole representation, KNS Spring Meeting, Jeju, Korea, 2015
5. C. Josey, P. Ducru, B. Forget, K. Smith, Windowed multipole for cross section Doppler broadening, J. Comput. Phys. **307**, 715 (2016)
6. F.B. Brown, *The MAKXSF Code with Doppler Broadening. LA-UR-06-7002* (Los Alamos National Laboratory, 2006)
7. M. Lemaire, H. Lee, B. Ebiwonjumi, et al. Verification of photon transport capability of UNIST Monte Carlo code MCS, Comput. Phys. Commun. **231**, 1 (2018)
8. P.K. Romano, B. Forget, Parallel fission bank algorithm in Monte Carlo criticality calculations, Nucl. Sci. Eng. **170**, 125 (2012)
9. B.C. Kiedrowski, F.B. Brown, P.P.H. Wilson, Adjoint-weighted tallies for k-eigenvalue calculations with continuous-energy Monte Carlo, Nucl. Sci. Eng. **168**, 226 (2011)
10. E. Jeong, D. Lee, Development status of MCS Monte Carlo dynamics code for reactor transient analysis, RPHA 2023, Gyeongju, South Korea, October 24–26, 2023
11. M. Imron, D. Lee, Multi-physics Monte Carlo simulation for a pin-cell with continuous temperature and density, RPHA 2023, Gyeongju, South Korea, October 24–26, 2023
12. M. Pusa, J. Leppänen, Computing the matrix exponential in burnup calculations, Nucl. Sci. Eng. **164**, 140 (2010)
13. A. Isotalo, V. Sahlberg, Comparison of neutronics-depletion coupling schemes for burnup calculations, Nucl. Sci. Eng. **179**, 434 (2015)
14. D. Lee, J. Rhodes, K. Smith, Quadratic depletion method for gadolinium isotopes in CASMO-5, Nucl. Sci. Eng. **174**, 79 (2013)
15. A.E. Isotalo, J. Leppänen, J. Dufek, Preventing xenon oscillations in Monte Carlo burnup calculations by enforcing equilibrium xenon distribution, Ann. Nucl. Energy **60**, 78 (2013)
16. M. Ryu, Y.S. Jung, H.H. Cho, H.G. Joo, Solution of the BEAVRS benchmark using the nTRACER direct whole core calculation code, J. Nucl. Sci. Technol. **52**, 961 (2015)
17. R.K. Salko, *CTF Theory Manual* (Reactor Dynamics and Fuel Management Group, Pennsylvania State University, 2014)
18. D.J. Kelly, T.M. Sutton, S.C. Wilson, MC21 analysis of the nuclear energy agency Monte Carlo performance benchmark problem, PHYSOR 2012, Knoxville, Tennessee, USA, April 15–20, 2012
19. T.D.C. Nguyen, H. Lee, S. Choi, D. Lee, Validation of UNIST Monte Carlo code MCS using VERA progression problems, Nucl. Eng. Technol. **52**, 878 (2020)
20. T.D.C. Nguyen, H. Lee, S. Choi, D. Lee, MCS/TH1D analysis of VERA whole-core multi-cycle depletion problems, Ann. Nucl. Energy **139**, 107271 (2020)
21. J. Jang, W. Kim, S. Jeong, E. Jeong, J. Park, M. Lemaire, H. Lee, Y. Jo, P. Zhang, D. Lee, Validation of UNIST Monte Carlo code MCS for criticality safety analysis of PWR spent fuel pool and storage cask, Ann. Nucl. Energy **114**, 495 (2018)
22. T.D. Long, S.G. Hong, D. Lee, Validation of UNIST Monte Carlo code MCS for criticality safety calculation with burnup credit through MOX criticality benchmark problem, Nucl. Eng. Tech. **53**, 19 (2021)
23. H. Lee, J. Jang, H. Kang, W. Kim, J. Jang, D. Lee, H.C. Lee, Criticality benchmark of Monte Carlo code MCS for light water reactor fuel in transportation and storage packages, Ann. Nucl. Energy **151**, 107873 (2021)
24. F. Setiawan, M. Lemaire, D. Lee, Analysis of VVER-1000 mock-up criticality experiments with nuclear data library ENDF/B-VIII.0 and Monte Carlo code MCS, Nucl. Eng. Tech. **53**, 1 (2021)
25. T.Q. Tran, J. Choe, X. Du, H. Lee, D. Lee, Neutronic simulation of China experimental fast reactor start-up tests-part II: MCS code Monte Carlo calculation, Ann. Nucl. Energy **148**, 107710 (2020)
26. T. Umbar, D. Lee, First criticality and uncertainty analysis of the HTR-PM using MCS, KNS Spring meeting, Jeju, South Korea, May 18–19, 2023
27. J. Yu, H. Lee, M. Lemaire, H. Kim, P. Zhang, D. Lee, MCS based neutronics/thermal-hydraulics/fuel-performance coupling with CTF and FRAPCON, Comput. Phys. Commun. **238**, 1 (2019)

28. J. Yu, H. Lee, H. Kim, P. Zhang, D. Lee, Coupling of FRAPCON for fuel performance analysis in the Monte Carlo code MCS, Comput. Phys. Commun. **251**, 106748 (2020)
29. J. Yu, H. Lee, H. Kim, P. Zhang, D. Lee, Coupled N-T/H simulation of BEAVRS cycle 1 depletion by MCS/CTF code system, Nucl. Technol. **206**, 728 (2020)
30. J. Yu, H. Lee, H. Kim, P. Zhang, D. Lee, Simulation of BEAVRS benchmark cycle 2 depletion with MCS/CTF coupling system, Nucl. Eng. Technol. **52**, 661 (2020)
31. J. Yu, H. Lee, M. Lemaire, H. Kim, P. Zhang, D. Lee, Fuel performance analysis of BEAVRS benchmark cycle 1 depletion with MCS/FRAPCON coupling system, Ann. Nucl. Energy **138**, 107192 (2020)
32. K.J. Geelhood, W.G. *Luscher, FRAPCON-4.0: Integral Assessment* (Pacific Northwest National Laboratory, PNNL-19418, 2015)
33. T.D.C. Nguyen, H. Lee, D. Lee, Use of Monte Carlo code MCS for multigroup cross section generation for fast reactor analysis, Nucl. Eng. Technol. **53**, 2788 (2021)
34. T.Q. Tran, A. Cherezov, X. Du, D. Lee, Verification of a two-step code system MCS/RAST-F to fast reactor core analysis, Nucl. Eng. Technol. **54**, 1789 (2022)
35. T.D.C. Nguyen, T.Q. Tran, D. Lee, Coupled neutronics/thermal-hydraulics analysis of ANTS-100e using MCS/RAST-F two-step code system, Nucl. Eng. Technol. **55**, 4048 (2023)
36. T.D.C. Nguyen, D. Lee, Group constants generation by Monte Carlo code MCS for LWR analysis, Comput. Phys. Commun. **285**, 108642 (2023)
37. P. Zhang, M. Lemaire, H. Lee, N. Mai, D. Lee, Development of a variance reduction scheme in the MCS Monte Carlo code, Transactions of Korean Nuclear Society Autumn Meeting, Yeosu, Korea, October 25–26, 2018
38. M. Lemaire, H. Lee, D. Lee, Implementation of tally convergence tests in UNIST Monte Carlo code MCS, Transactions of Korean Nuclear Society Autumn Meeting, Yeosu, Korea, October 25–26, 2018
39. N.N.T. Mai, P. Zhang, M. Lemaire, B. Ebiwonjumi, W. Kim, H. Lee, D. Lee, Extension of Monte Carlo code MCS to spent fuel cask shielding analysis, Int. J. Energy Res. **44**, 8089 (2020)
40. M. Lemaire, H. Lee, P. Zhang, D. Lee, Interpretation of two SINBAD photon-leakage benchmarks with nuclear library ENDF/B-VIII.0 and Monte Carlo code MCS, Nucl. Eng. Technol. **52**, 1355 (2020)
41. X.Y. Feng, P. Zhang, H. Lee, D. Lee, H.C. Lee, Validation of MCS code for shielding calculation using SINBAD, Nucl. Eng. Technol. **54**, 3429 (2022)
42. Y. Jo, D. Lee, A study on effect of assembly power history to gamma dose rate in spent fuel pool at a short cooling time, Transactions of Korean Nuclear Society Spring Meeting, Jeju, Korea, May 18–19, 2023
43. ICRP, Conversion coefficients for radiological protection quantities for external radiation exposures, ICRP Publication 116, Ann. ICRP **40(2-5)** (2010)
44. Korea Electric Power Corporation and Korea Hydro & Nuclear Power Co., Ltd., APR1400 Design control document tier 2 - Chapter 12 radiation protection, US NRC, 2018
45. Design requirements for light water reactor fuel handling systems, ANSI/ANS 57.1-1992
46. Y. Jo, C. Kong, A. Cherezov, D. Lee, Sensitivity and uncertainty analysis capability in MCS for UAM benchmark. M&C 2019, Oregon USA, August 25–29, 2019
47. Y. Jo, V. Dos, N.N.T. Mai, H. Lee, D. Lee, Uncertainty analysis of sub-exercises in UAM-SFR benchmark with the MCS code, EPJ Web Conf. **247**, 15017 (2021)
48. M.L. Williams, *CRC Handbook of Nuclear Reactors Calculations, Vol. III, Perturbation Theory for Nuclear Reactor Analysis* (CRC Press, Inc., Boca Raton, 1986)
49. H.J. Shim, C.H. Kim, Adjoint sensitivity and uncertainty analyses in Monte Carlo forward calculations. J. Nucl. Sci. Technol. **48**, 1453 (2011)
50. S.H. Choi, H.J. Shim, C.H. Kim, Development of generalized perturbation theory algorithms for Monte Carlo eigenvalue calculations, Nucl. Sci. Eng. **189**, 171 (2018)
51. Y. Qiu, X. Shang, X. Tang, J. Liang, K. Wang, Computing eigenvalue sensitivity coefficients to nuclear data by adjoint superhistory method and adjoint Wielandt method implemented in RMC code, Ann. Nucl. Energy **87**, 228 (2016)
52. T. Yamamoto, Eigenvalue sensitivity analysis capabilities with the differential operator method in the superhistory Monte Carlo method, Ann. Nucl. Energy **112**, 150 (2018)
53. F.B. Brown, Wielandt acceleration for MCNP5 Monte Carlo eigenvalue calculations. Joint International Topical Meeting on Mathematics & Computation and Supercomputing in Nuclear Applications (M&C+ SNA 2007), Monterey, California, 2007
54. S.H. Choi, H.J. Shim, Memory-efficient calculations of adjoint-weighted tallies by the Monte Carlo Wielandt method, Ann. Nucl. Energy **96**, 287 (2016)
55. J. Leppänen, M. Pusa, T. Viitanen, V. Valtavirta, T. Kaltiaisenaho, The Serpent Monte Carlo code: Status, development and applications in 2013, Ann. Nucl. Energy **82**, 142 (2015)
56. M. Aufiero, A. Bidaud, M. Hursin, J. Leppänen, G. Palmiotti, S. Pelloni, P. Rubiolo, A collision history-based approach to sensitivity/perturbation calculations in the continuous energy Monte Carlo code SERPENT, Ann. Nucl. Energy **85**, 245 (2015)
57. Y. Jo, D. Lee, Development of an adjoint flux calculation technique for exact perturbation theory in Monte Carlo code MCS. In SNA + MC 2024, Paris, France, October 20–24, 2024

Cite this article as: Yunki Jo, Deokjung Lee. Current capabilities and future developments of Monte Carlo code MCS, EPJ Nuclear Sci. Technol. **11**, 7 (2025). https://doi.org/10.1051/epjn/2025001.